Are Spherulitic Lacustrine Carbonates an Expression of Large-Scale Mineral Carbonation? A case study from the East Kirkton Limestone, Scotland.

Mike Rogerson[1], Ramon Mercedes-Martín[1], Alexander T. Brasier[2], Rona A.R. McGill[3], Tim J. Prior[4], Hubert Vonhof[5], Simon M. Fellows[4], John J. G. Reijmer[6], Erin McClymont[7], Ian Billing[8,9], Anna, Matthews[8] and Martyn Pedley[1]

1. Department of Geography, Environment and Earth Sciences, University of Hull, Cottingham Road, Hull, UK. HU6 7RX. Tel. +44 (0)1482466051. m.rogerson@hull.ac.uk; r.mercedes@hull.ac.uk; h.m.Pedley@hull.ac.uk

2. School of Geosciences, Meston Building, University of Aberdeen, Old Aberdeen, Scotland, UK. AB24 3UE. Tel. +44(0)1224273449. a.brasier@abdn.ac.uk

3. Scottish Universities Environmental Research Centre (SUERC), Rankine Avenue, East Kilbride G75 0QF. Tel. +44(0) 01355270158. Rona.McGill@glasgow.ac.uk

4. Department of Chemistry, University of Hull, Cottingham Road, Hull, UK. HU6 7RX. Tel. +44(0)1482466389. t.prior@hull.ac.uk; s.m.fellows@hull.ac.uk

5. Max Planck Institute of Chemistry, Hahn-Meitnerweg 1, 55128, Mainz Germany. Tel +4961313056605. hubert.vonhof@mpic.de

6. Faculty of Earth and Life Sciences, Vrije Universiteit Amsterdam, De Boelelaan 1085, 1081HV, Amsterdam, The Netherlands. 1081HV. Tel. +31 20 59 87360. h.b.vonhof@vu.nl; j.j.g.reijmer@vu.nl

7 Department of Geography , Durham University , Lower Mountjoy , South Road, Durham , DH1 3LE, UK

8 BP Exploration - Integrated Subsurface Description & Modelling, Bldg H, Desk W172 Chertsey Road, Sunbury on Thames, TW16 7LN

9 University of Derby, Kedleston Road , Derby, DE22 1GB

ABSTRACT

Lacustrine carbonate deposits with spherulitic facies are poorly understood, but are key to understanding the economically important "Pre-Salt" Mesozoic strata of the South Atlantic. A major barrier to research into these unique and spectacular facies is the lack of good lacustrine spherulite-dominated deposits which are known in outcrop. Stratigraphy and petrography suggest one of the best analogue systems is found in the Carboniferous of Scotland: the East Kirkton Limestone. Here we propose a hydrogeochemical model that explains why the $CaCO_3$, SiO_2, Mg-Si-Al mineral suite associated with spherular radial calcite facies forms in alkaline lakes above basaltic bedrock. Demonstrating links between igneous bedrock chemistry, lake and spring water chemistry and mineral precipitation, this model has implications for studies of lacustrine sediments in rift basins of all ages. Using empirical and theoretical approaches, we analyze the relationship between metal mobilization from sub-surface volcaniclastic rocks and the potential for precipitation of carbonate minerals,

various Mg-bearing minerals and chalcedony in a lacustrine spherulitic carbonate setting. This suite of minerals is most likely formed by in-gassing of CO_2 to a carbon-limited alkaline springwater, consistent with the reaction of alkali igneous rocks in the subsurface with meteoric groundwater. We suggest that an analogous system to that at East Kirkton caused development of the 'Pre-Salt' spherulitic carbonate deposits.

Keywords: Palaeozoic, magnesium silicate, calcite, hydrolysis, Pre-Salt, palaeogeography, lake, PHREEQC, Europe, Sediment mineralogy

1. INTRODUCTION

Fibro-radial spherulitic calcite components are relatively well known on a small scale from vadose, lacustrine and marine environments (Verrecchia et al., 1995; Braissant et al., 2003; Arp et al., 2012; Wanas, 2012; Casado et al., 2014; Bahniuk et al., 2015). However, deposits constituted of more than a few grains of spherulitic habit are rare, and probably limited to specific processes and depositional conditions that are currently poorly constrained. Comparatively little studied, there has been increasing interest in understanding how such voluminous lacustrine spherulitic calcite deposits, and the SiO_2 and Mg-Si-Al suite of minerals typically associated with them, were precipitated. This increased interest has been further motivated by the need to explain the economically-significant and spatially voluminous early Cretaceous 'Pre-Salt' carbonate reservoirs of Brazil and Angola (Wright, 2012; Wright and Barnett, 2015). The origin of these highly unusual deposits, which

63 occupied rift lakes formed during opening of the South Atlantic, is controversial (Wright,
64 2012; Mercedes-Martín et al., 2016).
65 Crucial first-order questions, such as the source(s) of the calcium and silica being deposited,
66 remain unanswered. The sheer masses of minerals precipitated from the Cretaceous lakes
67 imply a major mass-transfer process operated at the time, but this process has not been
68 identified. What is clear is that the petrographic appearances of these sediments is
69 markedly different from known Recent "meteogene" or "tufa" carbonate deposits (Wright,
70 2012). Equally, the very high volume of carbonate emplaced demonstrates that these
71 systems were not metal-limited as most modern "thermogene" or "travertine" deposits are
72 (Guido and Campbell, 2011; Renaut et al., 2013). Such geologically unusual deposits imply
73 an unusual mass transfer mechanism operated during rifting of the South Atlantic.
74

75 **1.1. Fibro-Radial Calcite and the Great Pre-Salt Controversy**

76 In the 'Pre-Salt' South Atlantic rift lake rocks, fibro-radial carbonate components 'float'
77 within Mg-rich clay deposits (Dias, 1998; Terra et al., 2010; Wright and Barnett, 2015). The
78 precise genetic relationship between these Mg-Si and $CaCO_3$ phases is a subject of ongoing
79 controversy that needs resolving if the origin of the 'Pre-Salt' deposits is to be elucidated
80 (Mercedes-Martín et al., 2016). Hypotheses based on petrographic observations variously
81 suggest fibro-radial calcite arises from displacive concretionary crystal growth within Mg-Si
82 matrices (Dorobek et al., 2012), or as early diagenetic features from Mg-Si gel catalysis
83 (Wright and Barnett, 2015) or as a consequence of crystal growth in the presence of specific
84 organic compounds (Mercedes-Martin et al, 2016). All three hypotheses are yet to be

rigorously experimentally tested, and a major barrier to effective testing is a lack of suitable deposits that can be investigated beyond proprietary and confidential drill core material of the South Atlantic rift lakes. Some partial analogues are known from the literature, for example minor spherulitic facies are reported from the distal facies of Jurassic hot spring systems from Deseado Massif, Argentina (Guido and Campbell, 2011). Here we focus on the mechanisms leading to the precipitation of carbonates and silicates in a lacustrine Carboniferous analogue from Scotland, UK.

1.2. The East Kirkton Limestone: an interesting case study of rifting-related spherulitic limestones

The Carboniferous East Kirkton Limestone of the Midland Valley graben of Scotland (Fig. 1) contains calcium carbonate spherulites, spherulitic bioherms, calcite-smectite laminites and primary chert (Rolfe et al., 1993; Walkden et al, 1993). It occurs as a Member of the upper part of the West Lothian Oil Shale Formation (Smith et al., 1993), and its petrology, paleontology, stratigraphy and isotope geochemistry were well described in studies from the 1980s and 1990s (Wood et al., 1985, McGill, 1994; McGill et al, 1994; Clarkson et al, 1993; Rolfe et al., 1993; Walkden et al., 1993; Goodacre, 1999). However, despite this significant effort to understand the East Kirkton Limestone, aspects of the system could not be elucidated two decades ago. A pivotal question lies in unravelling the source of the calcium and silica mass deposited in the lake, which is implicit in ongoing debates over whether the water in the lake was affected by deep-sourced “geothermal” springs (McGill et al., 1994).

The West Lothian Oil-Shale was deposited during a phase of rapid extension of the Midland Valley Basin, and these strata were strongly affected during their deposition by right lateral strike-slip movement which created half-grabens with tilted blocks forming inter-basin highs (Whyte, 1993; Read et al., 2002). Rift evolution was pulsed, with each phase of activity producing voluminous calc-alkaline extrusive igneous products (Monaghan and Parrish, 2006). These products were interbedded as volcaniclastic rocks below, within and above the East Kirkton Limestone, indicating that the lacustrine phase was short-lived and coincided with an active volcanic pulse.

Basins opened throughout the South Atlantic in the Mesozoic from the Berriasian, due to rifting followed by strong thermal subsidence (Karner et al., 2003). In the southern basins of interest to this study (Moulin et al., 2005), rifting was active from the Barremian to base Aptian (Chaboureau et al., 2013). The active rifting was characterised by widespread, largely trachytic, volcanism (Teboul et al., 2017) which was particularly voluminous in the southern sector, encompassing the Santos / Campo and South Kwanza basins (Chaboureau et al., 2013). The Pre Salt carbonate formations developed during Early Aptian as accommodation was created by thermal sag of these rift basins (Karner et al., 2003). Volcanism continued within the Santos (Moreira et al., 2007) and Campos (Rangel et al., 1994) basins into the Aptian, reflecting that some lithospheric stretching continued into the period of extensive carbonate deposition. As at East Kirkton, lacustrine carbonate formations are therefore underlain by thick calc-alkaline volcanic materials, and deposition is associated within minor ongoing extrusive volcanic activity.

Overall, the East Kirkton Limestone seems an exceptional case study to better understand the origin of the mineral phases developed in rift volcanic lake settings such as those forming the South Atlantic 'Pre-Salt' deposits (sensu Dias, 1998, and Terra et al., 2010). The East Kirkton Limestone is also an important geoheritage site in its own right, famous for being the place where the earliest known well-preserved amphibian reptile skeleton was discovered (*Westlothiana lizziae*; Wood et al., 1985), so our findings have inherent value in further constraining a globally important early reptilian habitat.

2. MATERIALS AND METHODS

The type section of the East Kirkton Limestone is a quarry face (Fig. 1), where a heavily silicified spring emergence zone occurs at the northern limit giving way to layered carbonate, chalcedony and volcaniclastic deposits on its southern edge. This deposit was logged and sampled in August 2014. In addition, a series of boreholes (BH1, BH2 and BH3) drilled during 1987 and 1988 from the immediate area around the quarry were accessed, logged and sampled via the BGS Core Repository at Keyworth (UK) in February 2015. In particular, borehole BH2 is comprised of thick altered volcaniclastics attributed to unit 61 of the East Kirkton Limestone (see Rolfe et al., 1993), and borehole BH3 hosts more than 60 cm-thick tuffaceous rocks. Geochemical analyses were performed from samples in borehole BH3.

2.1. Optical and Energy-Dispersive X-Ray Spectroscopy (EDS) analysis

Optical microscopic examinations of thin sections were made with a Nikon Microphot FX microscope interfaced with a Nikon DS-Fi2 camera, and Nikon Elements D software. An

151 Oxford Instruments Peltier-cooled type X-Max 80 EDS system integrated with a Zeiss EVO60
152 Scanning Electron Microscopy was used to determine the abundance of specific elements
153 through the X-rays energy spectrum. Rasterization of particular areas within the sample was
154 implemented to obtain the chemical abundance of elements and create from matrix points,
155 using a standard method within the INCA Energy software.

156 **2.2. X-ray powder diffraction**

157 X-ray powder diffraction data were collected from ground samples mounted in stainless
158 steel sample holders. A PANAlytical Empyrean diffractometer operating in Bragg-Brentano
159 geometry with copper Kα1 (λ = 1.540546 Å) and a PIXEL detector was used for the data
160 collection.

161 **2.3. Sr Isotopes**

162 The mobile fraction of strontium (i.e. HNO_3 soluble) from samples taken from within the
163 East Kirkton Limestone and from the altered igneous rocks of BH1 (Table 1) were extracted
164 from powdered samples in PFA Teflon (Savillex) beakers on a hotplate at 140-150^{o}C using
165 ultrapure HNO3. Analysis follows standard procedures (Henderson et al., 1994; Pin et al.,
166 1994) with multiple HNO_3 elutions from a Triskem Sr-spec resin packed Bio-Rad glass
167 column. Pure strontium concentrates were loaded on to Re filaments using Ta emitter
168 solution and analyses carried out on a VG sector 54-30 thermal ionisation Mass
169 spectrometer at SUERC.

170 **2.4. Organic Geochemistry**

171 Lipid biomarkers were extracted from c.2.8 – 4.0g of freeze-dried and homogenised sample,
172 following the microwave-assisted extraction methodology of Kornilova and Rosell-Melé

(2003). Known concentrations of 5α-cholestane and hexatriacontane (Sigma-Aldrich) were added as internal standards. Each total lipid extract was hydrolysed using 8% KOH in methanol, heated for 1 hr at 70ºC and left overnight. Neutral fractions were recovered using repeated liquid extraction with hexane, then separated into apolar, ketone and polar fractions using silica column chromatography and *n*-hexane, dichloromethane and methanol as eluents, respectively. The apolar fractions were analysed by gas chromatography-mass spectrometry (GC-MS), using a 30m HP-5MS fused silica column (0.25 mm i.d. 0.25µm of 5% phenyl methyl siloxane). The carrier gas was He, and the oven temperature was programmed as follows: 60-200oC at 20oC/min, then to 320oC (held 35 min) at 6^{o}C/min. The mass spectrometer was operated in full-scan mode (50-650 amu/s, electron voltage 70eV, source temperature 230^{o}C). Quantification was achieved through comparison of integrated peak areas in the total ion chromatograms and those of the internal standards. Known concentrations of 5α-cholestane and hexatriacontane (Sigma-Aldrich) were added as internal standards. Each lipid extract was hydrolysed using 8% KOH in methanol, heated for 1 hr at 70^{o}C and left overnight. Neutral fractions were recovered using repeated liquid extraction with hexane, then separated into apolar, ketone and polar fractions using silica column chromatography and n-hexane, dichloromethane and methanol as eluents, respectively. The apolar fractions were analysed by gas chromatography-mass spectrometry (GC-MS), using a 30m HP-5MS fused silica column (0.25 mm i.d. 0.25µm of 5% phenyl methyl siloxane). The carrier gas was He, and the oven temperature was programmed as follows: 60-200^{o}C at 20^{o}C/min, then to 320^{o}C (held 35 min) at 6^{o}C/min. The mass spectrometer was operated in full-scan mode (50-650 amu/s, electron voltage 70eV, source

195 temperature 230^{o}C). Quantification was achieved through comparison of integrated peak
196 areas in the total ion chromatograms and those of the internal standards.
197
198 **3. RESULTS**
199 The general stratigraphy, mineralogy and geochemistry of the East Kirkton Limestone were
200 previously described by Clarkson et al., 1993; Rolfe et al., 1993; Smith et al., 1993; Walkden
201 et al., 1993; McGill et al, 1994; Goodacre, 1998. The most significant facies (Fig. 2, Fig. S1)
202 and a representative sedimentary facies log (borehole BH3, Fig. 3) are provided to illustrate
203 the main stratigraphic features. The mineral assemblages and stratigraphic context of these
204 deposits are comparable to those documented so far in the South Atlantic 'Pre-Salt' rift
205 lakes (*sensu* Bertani and Carozzi, 1985; Dias, 1998; Terra et al., 2010; Tosca and Wright,
206 2015; Saller et al., 2016). We make this claim on the basis of: i) the occurrence of meter-
207 scale beds yielding abundant partially eroded fibro-radial, spherical calcite components
208 about 1mm in size and displaying sweeping extinction; ii) the presence of serpentine-rich
209 floatstone of spherulitic components; iii) the laminated nature of the alternations of Mg-Si
210 and $CaCO_3$ mineral phases throughout; and the presence of significant chalcedony and
211 calcite cementing both Mg-Si and Ca phases (Fig. 4), iv) presence of mature hydrocarbons
212 stored in spherulitic biohermal reservoir facies (Fig. S1F).
213
214 Thin section and XRD analyses (Figs. 4 and 5) both demonstrate that the primary carbonate
215 mineralogy is dominantly calcite, with silica and dolomite as secondary phases: the
216 composition and mineral paragenesis of this rock is consistent with currently published data

on South Atlantic 'Pre-Salt' deposits (Bertani and Carozzi, 1985; Dias, 1998; Terra et al., 2010; Tosca and Wright, 2015; Saller et al., 2016). It is possibly coincidental that the East Kirkton Limestone contains abundant mature hydrocarbons (Fig. 6), which have likely migrated into this reservoir facies from the black lacustrine West Lothian Oil-shale, however this does illustrate that it occurs in a hydrocarbon-prone basin context analogous to the Pre Salt and that migration of mature hydrocarbons and their formation waters are shared features of the paragenesis of both deposits.

3.1. Stratigraphic relationships

Borehole BH-3 (Fig. 3) displays a soil and rock cover in the first 3 m. Spherulitic carbonates are found between 2.8 and 3.6 m and between 4.3 and 6.2 m depth occuring as laminites, which are formed by the alternation of carbonate-rich and organic-rich laminae hosting abundant calcite spherulitic components (Fig. 2B, C; Fig. S1A, B). In some cases, a large number of spherulites are found floating in clay/organic to mudstone-rich matrices producing floatstone textures (Fig. 2D). Soft-sediment deformation (slumps, creeping of laminae, Fig. 2A, Fig. S1B) and diverse biota is occasionally recognised in laminites (Fig. S1C). Some cm-scale calcareous-rich tuff layers are interbedded within the sequence (from 3.6 to 3.8m depth, Fig. S1D) which hardly ever contains spherulitic components. Three organic-rich shale packages (3.8 to 4.3 m; 6.2 to 7.3 m, and 7.8 to 13.5 m depth) previously named Little Cliff Shale Member by Rolfe et al., (1993) are also recorded. These authors identified pelecypods (*Curvirimula scotica*), plants (*Lepidodendron*), fish scales, ostracods (*Carbonita*),

238 and arthropods. A 50cm-thick layered carbonate interval (Fig. 3A) is recorded between 7.3
239 and 7.8 m depths displaying nodular to tabular beds of wackestone to floatstone textures.
240 Evidence of slumps and convolute beds is present and peloids, fish scales and ostracods
241 allochems are common. In the bottom of the borehole (between 13.5 and 14.6 m depth) a
242 greenish to dark orange tuff is recognised (Fig. 3, Fig. S1D). This unit is characterised by a
243 pyroclastic texture with mm-thick angular to subangular lapilli clasts surrounded by fine-
244 grained vesicular and amygdaloidal ash and shards (Fig. S1D). In some cases, calcite
245 pseudomorphs after altered amygdale textures were observed emplaced within plagioclase
246 or olivine phenocrysts (Fig. 2E), and some of these alkali minerals showed alteration
247 textures to serpentine-like clay minerals. In addition, centimetre-sized irregular cavities
248 filled with sequential generations of fibroradial/spherulitic chalcedony and drusy
249 megaquartz cements (Fig. 2F) are also present in some spherulitic biohermal carbonate
250 units (not shown in the log, Fig. S1F)..

251

252 **3.2. Petrological observations**

253 XRD analyses of the tuffs underlying the East Kirkton section indicate they have now
254 completely replaced to calcite (Fig. 5A). The spatially-resolved EDS map of the altered tuff
255 (across the white square in Fig. 5A) shows that pure calcite cement occurs as a light
256 coloured fabric under plane-polarized light (top left in Fig. 3A, corresponding to high
257 concentrations of Ca in Fig. 5B). A greenish brown area rich in Al, Mg and Fe (center and top-
258 right in Fig. 5A, corresponding to high concentrations of these elements in Fig. 5B) is a

serpentine-like clay alteration product (Fig. 5C), similar to that encountered in the lacustrine deposits located higher in the East Kirkton stratigraphy (Fig. 5). A pale green region in the bottom left (Fig. 5A) is rich in K and Al and likely contains un-altered components of the original feldspar mineral phase.

3.3. Strontium isotope data

Results of strontium isotope analysis (Fig. 7) demonstrate that a substantial component of this metal was ultimately derived from a mantle source. Also, comparison with the BH3 material and published data for the Midland Valley volcanic rocks indicate that BH3 volcanic tuffs and the lacustrine carbonate deposit are geochemically compatible, and probably co-developed, whereas both are less radiogenic than the original volcanic rocks.

4. DISCUSSION

Overall, the tectono-stratigraphic context and mineral paragenesis recognised at East Kirkton are compellingly similar to the Pre-Salt deposits, representing a unique opportunity to study the hydrogeochemical processes enabling the development of these unusual deposits in detail. As with Pre Salt deposits, we interpret the East Kirkton deposit as an alkaline lake fed by springs with a high dissolved mass. Interpretation that the East Kirkton Limestone formed in an alkaline lake fed by a hot-spring are not new (McGill et al., 1993; Walkden et al., 1993). However, no previous study has been able to deduce the origin of the carbonate and silica-rich solutions contributing to the lake water mass. Here we present new petrographical analyses showing that the tuff in borehole BH3 underlying the

Limestone deposit (Fig. 3, Fig. 5, and S1D) displays textural and chemical evidence of replacement and alteration (Fig. 2E, 5) and only a faint geochemical signature of the original mineralogy can be identified. This alteration moved the $^{87}Sr/^{86}Sr$ ratio away from the composition of unaltered regional igneous rocks, towards a composition also seen in the spherulitic carbonate deposits vertically above (Fig. 7). We infer that these two systems were in connection, and that the altering water was derived from meteoric input (Walkden et al., 1993).

The composition of Midland Valley Carboniferous extrusive igneous rocks nearby (Monaghan and Parrish, 2006) indicate that the original mineralogy of this material was a fairly standard pyroxene-olivine-feldspar assemblage, and this is compatible with the remnant Mg, Fe, K, Al found within the weathered tuffs (Fig. 5). The dominance of Ca in the weathered residue indicates that the feldspars were close to the anorthite end member and the pyroxenes were close to the Ca-rich end member in the original mineralogy. These minerals are known to be prone to weathering by infiltrating water, and undergo the following hydrolysis reactions (Equations 1-3), which are essentially the metasomatic reactions involved in serpentinization (Müntener, 2010; Hövelmann et al., 2011).

1. **Clinopyroxene** $Ca_2Si_2O_{6(s)} + 2H_2O_{(l)} \rightleftharpoons 2Ca^{2+}_{(aq)} + 2SiO_{2(aq)} + 4OH^-_{(aq)}$
2. **Anorthite** $Ca_2Al_2Si_2O_{8(s)} \rightleftharpoons 2Ca^{2+}_{(aq)} + 2AlO^-_{2(aq)} + 2SiO_{2(aq)}$
3. **Olivine** $MgFeSiO_{4(s)} + 2H_2O_{(l)} \rightleftharpoons Mg^{2+}_{(aq)} + Fe^{2+}_{(aq)} + SiO_{2(aq)} + 4OH^-_{(aq)}$

In all three reactions, the dissolved products cause hydrolysis resulting in very alkaline solutions. Ultimately, the solution produced by these reactions: i) will have a very high pH; ii) will be reducing; iii) will be rich in Ca, Si, Al, Mg and Fe. The molar ratios of fluid reaching the Earth's surface will be determined by 1) the molar ratios in the original rock, and 2) the molar ratio of secondary precipitates left by the solution in the subsurface.

The abundance of carbonate secondary precipitates in BH1 (Fig. 5) shows that the precipitating fluid contained substantial amounts of dissolved inorganic carbon. This is common in both meteogene and thermogene settings (Pentecost, 2005), and results in significant deposition of carbonate minerals as observed in this case. Consequently, although the Midland Valley volcanic series can be expected to have contained >10% calcium by mass, springs reaching the surface having altered these rocks will be severely calcium-limited. This is observed in modern springs, even where pH has been raised above 10 by reactions analogous to equations 1-3 (Jones and Renaut, 2010; Renaut et al., 2013). To explain the Ca-rich spring implied by the spherulitic nature of the deposits at East Kirkton (Wright and Barnett, 2015; Mercedes-Martín et al., 2016), and more dramatically the exceptionally large mass of calcium deposited within the Pre-Salt Formations (Dias, 1998; Terra et al., 2010), such calcium limitation cannot have occurred, and the amount of calcium available to the subsurface fluids must have exceeded the capacity of the dissolved carbon supply to remove it. This implies that the waters were not geothermally sourced but were meteoric, and that the whole East Kirkton system was consuming very large masses of carbon derived from the atmosphere. Large-scale geochemical systems fulfilling this

description occur today within exhumed ophiolites, for example the Somail Ophiolite in Oman (Matter and Kelemen, 2009). Springs fed from carbon-limited reactions in the subsurface have led to the deposition of an estimated 10^7 m^3 of carbonate on the surface, covering an area of ~200,000 m^2, in the last ~50,000 years alone (Kelemen and Matter, 2008). We propose that an analogous geochemical system led to the development of both the East Kirkton and Pre-Salt carbonate formations.

4.1. Understanding a Carbon-Limited, Hyperalkaline Spring System

On emergence at the surface, a carbon-limited solution produced by weathering alkaline tuff would rapidly equilibrate by reacting with atmospheric $CO_{2\,(g)}$ to produce a range of mineral products. Summatively, reactions 1-3 and 4 result in a balanced transfer of mass from clinopyroxene, olivine and feldspar to calcite, silica and serpentine-like clay (stevensite at high pH and high Mg/ Si ratios; Tosca and Masterton, 2014) and Mg-Al phases, and these reactions are essentially identical to those reported from weathering ophiolite systems (Kelemen and Matter, 2008).

4. $$Ca_2Si_2O_{6(s)} + Ca_2Al_2Si_2O_{8(s)} + 3MgFeSiO_{4(s)} + 4.5H_2O_{(l)} + 11CO_{2(g)} \rightleftharpoons 4CaCO_{3(s)} + 3SiO_{2(s)} + 1.5Fe_2O_{3(s)} + Mg_3Si_4O_{10}(OH)_{2(s)} + 2AlO^-_{2(aq)} + 7HCO^-_{3(aq)}$$

Our hypothesis is that there is no geothermal heating from active magma systems from which excess CO_2 could be provided, however this does not imply the spring was necessarily cold. Reactions 1-4 are exothermic (Wenner and Taylor, 1971), so it is likely the waters

346 arising from them were warm. Temperatures as high as 60°C for the East Kirkton lake water
347 have been inferred from $\delta^{18}O$ in silica (McGill et al, 1993). We note that Walkden et al.
348 (1993) estimated an average lake temperature of 20°C from oxygen isotopes in calcite
349 spherules, however this facies may reflect a distal setting in which significant dissolved
350 organic matter was present in solution (Mercedes-Martin et al., 2016) as reported in
351 Patagonia (Guido and Campbell, 2011). The high-temperature siliceous facies and the low-
352 temperature spherulite facies are therefore compatible with relatively high (proximal) and
353 low (distal) spring influence respectively. In any case, the importance of identifying whether
354 the water was hot or cold derives, in large part, from the value of raised temperature as a
355 proxy for a non-karstic source for the calcium and carbonate ions. Our analysis indicates
356 that these ions were sourced from igneous rock weathering regardless of spring water
357 temperature, and so the emphasis on understanding temperature is much reduced.
358
359 The evolution of the solution, and the paragenesis of depositional products derived from it,
360 can be explored by sequentially exposing a spring representative of carbon-limited reactions
361 1-3 to $CO_{2(g)}$ at surface conditions using a simple thermodynamic approach via PHREEQC
362 modelling (Parkhurst and Appelo, 1999; Fig. 8, See Supplementary Material). Here, we use a
363 representative springwater from the Somail Ophiolite (see Supplementary material). We
364 find that Mg-Si phases are most insoluble initially; $CaCO_3$ phases precipitate in almost
365 stoichiometric balance with the ingassing of carbon dioxide; and SiO_2 phases increase in
366 insolubility as pH falls (Fig. 8). Indeed, by allowing the system to achieve equilibrium with
367 excess CO_2, we can also investigate the predicted paragenesis for the mineral assemblage.

368 Figure 4 shows that with increasing ingassing, serpentine-like Mg-Si phases remineralize to a
369 combination of Mg-Al phases and dolomite as $OH^-_{(aq)}$ becomes unavailable below the pH ~10
370 transition, which is consistent with paragenesis concepts for the Pre-Salt (Wright and
371 Barnett, 2015). Simultaneous deposition of calcite, silica, dolomite and serpentine-like clays
372 around the lake shores implies an equilibrium pH of ~8 for lake waters (Fig. 8), comfortably
373 within the range of modern alkaline surface waters (Rogerson et al., 2014). Alternation of
374 calcite- and silica-dominated phases in the more distal lake environments in this case is
375 consistent with an oscillation of water chemistry around pH 7, presumably reflecting
376 variable balance in the input flux of spring and ambient meteoric water. However, this result
377 is unlikely to be unique and may reflect the specific chemistry of the spring system itself.
378 The diagenetic changes implied by the succession of Mg-phases in Figure 8 indicate that
379 secondary porosity is likely to develop. This is consistent with the behaviour of Mg-Si in the
380 Pre-Salt system as more fully developed by Tosca and Wright (2015).
381
382 **4.2. Is Carbon-limited Mass Transfer to Terrestrial Carbonates a Significant Sediment**
383 **Transport Process?**
384 The similarity of the sediments and mineral phases at East Kirkton to those of the larger
385 South Atlantic Cretaceous lakes implies a strong similarity in their genetic processes, and
386 therefore that similar mass-transfer geochemical processes are likely to have been
387 operating on a very large scale in the early Mesozoic. Indeed, the geochemical signature of
388 subsurface alteration of this type has also been reported for the igneous series underlying
389 the 'Pre-Salt' carbonates. During rainy periods chemical weathering of basic volcaniclastic

390 rocks and basaltic magmas is thought to have promoted an active transport of dissolved
391 cations (Na, Ca, K, Mg) into the Lagoa Feia lake ('Pre-Salt', Brazil; Bertani and Carozzi, 1985).
392 In addition, extensive calcitization processes and trioctahedral smectite formation took
393 place in the distal parts of the lacustrine terrigenous flats (Bertani and Carozzi, 1985).
394 Serpentinization of the exhumed mantle in several Brazilian 'Pre-Salt' basins can have
395 occurred down to depths of 6-8 km at the continental-oceanic crustal transition (Zalán et al.,
396 2011), providing an enormous reservoir of dissolved cations from igneous source rocks for
397 remobilisation in the 'Pre-Salt' lakes. Recent re-evaluation of the igneous series underlying
398 the Kwanza Pre-Salt basin offshore of Angola again indicates meteoric alteration, and
399 development of metal-rich fluids (Teboul et al., 2017). Our hypothesis only requires that this
400 alteration is done by relatively carbon-poor meteoric waters so that subsurface reactions
401 were carbon-limited not calcium-limited. In the case of the Kwanza basin, this is consistent
402 with low temperature alteration yielding highly alkaline, Mg, Ca and Si-rich solutions and
403 may have occurred early during alteration (Teboul et al., 2017). Later fluids, and thus
404 equilibrium mineral phases in the altered igneous rocks, indicate high-temperature
405 alteration from fluids rich in CO_2 (Teboul et al., 2017).
406 The primary difference between the East Kirkton deposit (spatial scale ~100's m) and Pre
407 Salt systems (~100s km) is scale, and some care in needed before mass transfer processes
408 can be assumed to apply over 3 orders of magnitude. However, as the scale of the lake
409 system being considered increases the potential to capture increasing numbers of large
410 spring systems also increases. It is clearly impossible that a Pre Salt system could be fed by a
411 single point source, as appears to be the case in East Kirkton. However, we see no reason

why multiple sources cannot be sufficient to condition a large lake watercolumn chemistry just as a single source conditions a small one. The primary difference will be multiple, potentially independently evolving, points of calcium, magnesium and silica supply to the lake to be active, likely giving rise to complex spatial and temporal variability in sedimentary facies and early diagenesis.

If this hypothesis if correct, the subsurface mass-transfer through pumping of aqueous solutions described at East Kirkton is capable of acting over scales of hundreds of kilometres. This is a basin-scale sedimentary process that has received very scant investigation, but may be repeated and predictable in basins where rapid extension and volcanic exhumation is taking place with dominantly low-lying, terrestrial conditions at the surface. We propose the East Kirkton Limestone as a type system for further investigation of this new carbon-limited mass transfer and depositional systems associated with subsurface alkaline rock weathering.

5. CONCLUSIONS

We hypothesise that the East Kirkton Limestone is the depositional end of a little recognised mass-transfer process originating with subsurface geochemical alteration of alkaline igneous volcanic rocks, acting through carbon-limited spring systems, which may have been heated by the reactions themselves, and terminating in potentially basin-scale lacustrine deposition in which minerals are formed from the mixture of spring water and atmospheric carbon. Today, this process occurs within exhumed ophiolites but may also be associated with a specific phase during crustal extension. The East Kirkton lithofacies and mineral assemblages

(carbonates, Mg-Si phases, and chalcedony) are so analogous to, and the geological background so coherent with, the South Atlantic Cretaceous 'Pre-Salt' strata that we conclude that similar processes are likely to have been acting there. Understanding the mass-transfer dynamics of hydrochemical systems in the subsurface will be fundamental to a process-based understanding of the origin of the spherical-radial carbonate phases recorded both at East Kirkton and in the 'Pre-Salt' deposits, and forms an intriguing new perspective on both the fate of metal mass remobilisation from extrusive igneous processes in these contexts and the geothermal significance of alkaline warm and hot springs.

ACKNOWLEDGEMENTS

BP Exploration Co. is thanked for funding, and particularly the Carbonate Team for supporting this research and for fruitful discussions. West Lothian Council and Scottish Natural Heritage are thanked for allowing access and permission for sampling the site. The Core Store Team at BGS Keyworth is particularly acknowledged for their assistance. Mark Anderson, Tony Sinclair (University of Hull), and Bouk Lacet (VU University Amsterdam) are thanked for technical support. Anne Kelly (SUERC) for carrying out the Strontium Isotope analyses. Mark Tyrer is thanked for his advice on PHREEQC modelling.

REFERENCES CITED

Arp, G., Helms, G., Karlinska, K., Schumann, G., Reimer, A., Reitner, J., and Trichet, J., 2012, Photosynthesis versus exopolymer degradation in the formation of microbialites on the

456 atoll of Kiritimati, Republic of Kiribati, Central Pacific: Geomicrobiology Journal, v. 29, no.
457 1, p. 29-65.
458 Bahniuk, A.M., Anjos, S., França, A. B., Matsuda, N., Eiler, J., McKenzie, J. A., and
459 Vasconcelos, C., 2015, Development of microbial carbonates in the Lower Cretaceous
460 Codó Formation (north-east Brazil): Implications for interpretation of microbialite facies
461 associations and palaeoenvironmental conditions: Sedimentology, v. 62, no. 1, p. 155-
462 181.
463 Bertani, R.T., and Carozzi, A.V., 1985. Lagoa Feia Formation (Lower Cretaceous) Campos
464 Basin, offshore Brazil: rift valley type lacustrine carbonate reservoirs – II: Journal of
465 Petroleum Geology, v. 8, no. 2, p. 199-220.
466 Braissant, O.,Cailleau, G., Dupraz, C., and Verrecchia, E.P., 2003. Bacterially induced
467 mineralization of calcium carbonate in terrestrial environments: the role of
468 exopolysaccharides and amino acids: Journal of Sedimentary Research, v. 73, p. 485-490.
469 Cameron, I. B., Aitken, A. M., Browne, M. A. E., Sephenson, D. (1998). Geology of the Falkirk
470 district: memoir for 1: 50 000 geological sheet 31E (Scotland). London, The Stationery
471 Office. 106pp.
472 Casado, A.I., Alonso-Zarza, A. M., and La Iglesia, A., 2014. Morphology and origin of dolomite
473 in paleosols and lacustrine sequences. Examples from the Miocene of the Madrid Basin:
474 Sedimentary Geology, v. 312, p. 50-62.
475 Chaboreau, A.C., Guillocheau, F., Robin, C., Moulin, M., Aslanian, D., 2013. Paleogeographic
476 evolution of the central segment of the South Atlantic during the Early Cretaceous times :
477 paleotopographic and geodynamic implications. Tectonophysics 604, 191-223.

478 Clarkson, E.N.K., Milner, A.R., and Coates, M.I., 1993. Palaeoecology of the Viséan of East
479 Kirkton, West Lothian, Scotland: Transactions of the Royal Society of Edinburgh: Earth
480 Sciences, v. 84, p. 417-425.
481 Dewandel, B., Lachassagne, P., Boudier, F., Al-Hatali, S., Ladouche, B., Pinault, J.-L., Al-
482 Suleimani, Z., 2005. A conceptual model of ophiolite hard-rock aquifers in Oman based
483 on a multiscale and a multidisciplinary approach. Hydrogeology Journal 13, 708-726.
484 Dias, L.J., 1998, Análise sedimentológica e estratigráfica do Andar aptiano em parte da
485 margem leste do Brasil e no platô das Malvinas: considerações sobre as primeiras
486 incursões e ingressões marinhas do oceano Atlântico Sul Meridional [Ph.D. thesis]: Brazil,
487 Universidade Federal do Rio Grande do Sul, 411p.
488 Dorobek, S., Piccoli, L., Coffey, B. and Adams, A., 2012. Carbonate rock-forming processes in
489 the Presalt “sag” successions of Campos Basin, offshore Brazil: evidence for seasonal,
490 dominantly abiotic carbonate precipitation, substrate controls, and broader geologic
491 implications: AAPG Hedberg Conference “Microbial Carbonate Reservoir
492 Characterization” Abstracts. Houston Texas.
493 Goodacre, I.R., 1999. Microbial carbonates in lacustrine settings: an investigation into the
494 Carboniferous East Kirkton Limestone [Ph.D. thesis]: Scotland, University of Aberdeen,
495 253p.
496 Guido, D.M., Campbell, K.A., 2011. Jurassic hot spring deposits of the Deseado Massif
497 (Patagonia, Argentina): Characteristics and controls on regional distribution: Journal of
498 Volcanology and Geothermal Research, v.203, 35-47.

499 Henderson, G., Martel, D., O'Nions, R., Shackleton, N., 1994. Evolution of seawater 87Sr86Sr
500 over the last 400 ka: the absence of glacial/interglacial cycles: Earth and Planetary
501 Science Letters, v.128, 643-651.
502 Hövelmann, J., Austrheim, H., Beinlich, A., and Anne Munz, A., 2011. Experimental study of
503 the carbonation of partially serpentinized and weathered peridotites: Geochimica et
504 Cosmochimica Acta, v.75, p. 6760-6779.
505 Jones, B., Renaut, R.W., 2010. Calcareous Spring Deposits in Continental Settings.
506 Sedimentology, v.61, 177-224.
507 Karner, G.D., Driscoll, N.W., Barker, D.H.N, 2003. Syn-rift region subsidence across the West
508 African continental margin; the role of lower plate ductile extension, In: Arthur, T.J.,
509 MacGregor, D.AS., Cameron, N.R. (Eds.), Geological Society of London, Special
510 Publications 207, 105-129
511 Kelemen, P.B., Matter, J., 2008. In situ carbonation of peridotite for CO2 storage.
512 Proceedings of the National Academy of Sciences, v.105, 17295-17300.
513 Matter, J.M., Kelemen, P.B., 2009. Permanent storage of carbon dioxide in geological
514 reservoirs by mineral carbonation. Nature Geoscience, v.2, 837-841.
515 McGill, R.A.R., 1994. Geochemistry and petrography of a Lower Carboniferous, lacustrine,
516 hot spring deposit: East Kirkton, Bathgate, Scotland [Ph.D. thesis]: Scotland, University of
517 Glasgow, 173p.
518 McGill, R.A.R., Hall, A.J., Fallick, A. E., and Boyce, A. J., 1994. The paleoenvironment of East
519 Kirkton, West Lothian, Scorland: stable isotope evidence from silicates and sulphides:
520 Transactions-Royal Society of Edinburgh: Earth Sciences v. 84, p. 223-237.

521 Mercedes-Martín, R., Rogerson, M., Brasier, A. T., Vonhof, H. B., Prior, T. J., Fellows, S. M.,
522 Reijmer, J.J.G., Billing, I., Pedley, H. M., 2016. Growing spherulitic grains in saline,
523 hyperalkaline lakes: experimental evaluation of the effects of Mg-clays and organic acids.
524 Sedimentary Geology v. 335, p. 93-102
525 Monaghan, A.A., and Parrish, R.R., 2006. Geochronology of Carboniferous-Permian
526 magmatism in the Midland Valley of Scotland: Implications for regional tectonomagmatic
527 evolution and the numerical time scale: Journal of the Geological Society v.163, p. 15-28.
528 Moreira, J.L.P., Madeira, C.V., Gil, J.A., Machado, M.A.P., 2007. Bacia de Santos. Boletim de
529 Geosciencias da Petrobras 15, 531-549.
530 Moulin, M., Aslanian, D., Olivet, J., Contrucci, I., Matias, L., Geli, L., Klingelhoefer, F., Nouze,
531 H., Rabineau, M., Labails, C., Rehault, J., Unternehr, P., 2005. Geological constraints on the
532 evolution of the Angolan margin based on reflection and refraction seismic data (ZaiAngo
533 Project). Geophysical Journal International 162, 793-810.
534 Müntener, O., 2010. Serpentine and serpentinization: a link between planet formation and
535 life: Geological Society of America, v. 38, no. 10, p. 959-960.
536 Palmer, M.R., Edmond, J.M., 1989. The Strontium Isotope Budget of the Modern Ocean.
537 Earth and Planetary Science Letters 92, 11-26.
538 Parkhurst, D.L., and Appelo, C A.J., 1999. User's guide to PHREEQC (Version 2): A computer
539 program for speciation, batch-reaction, one-dimensional transport, and inverse
540 geochemical calculations. 312 p.
541 Pentecost, A., 2005. Travertine. Springer, Berlin.

Pin, C., Briot, D., Bassin, C., Poitrasson, F., 1994. Concomitant separation of strontium and samarium-neodymium for isotopic analysis in silicate samples, based on specific extraction chromatography. Analytica Chimica Acta v. 298, 209-217.

Rangel, H.D., Martins, F.A.L, Esteves, F.R., Feijo, F.J., 1994. Bacia de Campos. Boletim de Geosciencias da Petrobras 8, 203-217.

Read, W.A., Browne, M.A.E., Stephenson, and D. Upton, B.J.G., 2002. Carboniferous, *in* Trewin, N. H., ed., The Geology of Scotland, 4th. Geological Society, London, p. 251–300.

Renaut, R.W., Owen, R.B., Jones, B., Tercelin, J.J., Tarits, C., Ego, J.K., Konhauser, K.O., 2013. Impact of lake-level changes on the formation of thermogene travertine in continental rifts: Evidence from Lake Bogoria, Kenya Rift Valley. Sedimentology, v.60, 428-468.

Rogerson, M., Pedley, M., Kelham, A. and Wadhawan, J., 2014, Linking mineralisation process and sedimentary product in terrestrial carbonates using a solution thermodynamic approach: Earth Surface Dynamics v. 2, p. 197-216.

Rolfe, W.D.I., Durant, G.P, Baird, W. J., Chaplin, C, Paton, R. L., and Reekie, R. J., 1993, The East Kirkton Limestone, Viséan, of West Lothian, Scotland: introduction and stratigraphy: Transactions of the Royal Society of Edinburgh: Earth Sciences, v. 84, no. 3-4, p. 177-188.

Saller, A., Rushton, S., Buambua, L., Inman, K., McNeil, R., & Dickson, J.T., 2016. Presalt stratigraphy and depositional systems in the Kwanza Basin, offshore Angola. AAPG Bulletin, 100(7), 1135-1164.

Smith, R.A., Stephenson, D. and Monro, S.K., 1993. The geological setting of the southern Bathgate hills, West Lothian, Scotland: Transactions of the Royal Society of Edinburgh: Earth Sciences, v. 4, no. 3-4, p.189-196.

564 Smedley, P.L., 1986. The relationship between calc-alkaline volcanism and within-plate
565 continental rift volcanism: evidence from Scottish Palaeozoic lavas. Earth and Planetary
566 Science Letters 77, 113-128.
567 Stanger, G., 1986. The hydrogeology of the Oman Mountains. Open University.
568 Teboul, P.-A., Kluska, J.-M., Marty, N.C.M., Debure, M., Durlet, C., Virgone, A., Gaucher, E.C.,
569 2017. Volcanic rock alterations of the Kwanza Basin, offshore Angola - Insights from an
570 integrated petrological, geochemical and numerical approach. Marine and Petroleum
571 Geology 80, 394-411.
572 Terra, G.J.S., Spadini, A.R., França, A.B., Sombra, C.L., Zambonato, E.E., Juschaks, L.C.d.S.,
573 Arienti, L.M., Erthal, M.M., Blauth, M., Franco, P.P., Matsuda, N.S., da Silva, N.G.C.,
574 Junior, P.A.M., D'Avila, R.S.F., deSouza, R.S., Tonietto, S.N., dos Anjos, S.M.C., Campinho,
575 V.S. and Winter, W.R., 2010, Classificação de rochas carbonáticas aplicável às bacias
576 sedimentares brasileiras: Bulletin Geoscience Petrobras, Rio de Janeiro, v.18, p. 9-29.
577 Tosca, N.J., and Wright, V.P., 2015. Diagenetic pathways linked to labile Mg-clays in
578 lacustrine carbonate reservoirs: a model for the origin of secondary porosity in the
579 Cretaceous pre-salt Barra Velha Formation, offshore Brazil, *in* Armitage, P. J., Butcher, A.
580 R., Churchill, J. M., Csoma, A. E., Hollis, C., Lander, R. H., Omma, J. E., and Worden, R. H.,
581 eds., Reservoir quality of clastic and carbonate rocks: analysis, modelling and prediction:
582 Geological Society, London, Special Publications, 435, SP435-1.
583 Veizer, J., Ala, D., Azmy, K., Bruckschen, P., Buhl, D., Bruhn, F., Carden, G.A.F., Diener, A.,
584 Ebneth, S., Goddéris, Y., Jasper, T., Korte, C., Pawellek, F., Podlaha, O.G., Strauss, H.,

585 1999. 87Sr/86Sr, 13C and 18O evolution of Phanerozoic seawater. Chemical Geology 161,
586 59-88.

587 Verrecchia, E. P, Freytet. P., Verrecchia, K. E., and Dumont, J-L., 1995, Spherulites in calcrete
588 laminar crusts: biogenic Ca CO_3 precipitation as a major contributor to crust formation:
589 Journal of Sedimentary Research, v. 65A, no. 4, p. 690-700.
590 Walkden, G. M., Roddy Irwin, J., and Fallick, A. E., 1993, Carbonate spherules and botryoids
591 as lake floor cements in the East Kirkton Limestone of West Lothian, Scotland:
592 Transactions of the Royal Society of Edinburgh: Earth Sciences, v. 84, no. 3-4, p. 213-221.
593 Wanas, H. A., 2012. Pseudospherulitic fibrous calcite from the Quaternary shallow lacustrine
594 carbonates of the Farafra Oasis, Western Desert, Egypt: A primary precipitate with
595 possible bacterial influence: Journal of African Earth Sciences, v. 65, p. 105–114.
596 Wenner, D.B., and Taylor, H.P., 1971. Temperatures of serpentinization of ultramafic rocks
597 based on O18/O16 fractionation between coexisting serpentine and magnetite:
598 Contributions to Mineralogy and Petrology, v. 32, no. 3, p.165-185.
599 Whyte, M. A., 1993. Scottish Carboniferous fresh-water limestones in their regional setting:
600 Transactions of the Royal Society of Edinburgh: Earth Sciences, v. 84, no.3-4, p. 239-248
601 Wood, S. P., Panchen, A. L. and Smithson, T. R., 1985. A terrestrial fauna from the Scottish
602 Lower Carboniferous: Nature, v. 314, p. 355-356.
603 Wright, V. P., 2012. Lacustrine carbonates in rift settings: the interaction of volcanic and
604 microbial processes on carbonate deposition, *in* Garland, L. E. Neilson, S. E., Laubach, and

605 Whidden, K. J., eds. Advances in carbonate exploration and reservoir analysis: Geological
606 Society, London, Special Publications 370, p. 39-47.
607 Wright, V. P., Barnett, A. J., 2015, An abiotic model for the development of textures in some
608 South Atlantic early Cretaceous lacustrine carbonates, *in* Bosence, D. W. J., Gibbons, K.
609 A., le Heron, D. P., Morgan, W. A., Pritchard, T. and Vining, B. A., eds. Microbial
610 Carbonates in Space and Time: Implications for Global Exploration and Production:
611 Geological Society, London, Special Publications 418, p. 209-219.
612 Zalán, P.V., Severino, M.D.C.G., Rigoti, C.A., Magnavita, L.P., and Bach, J.A., 2011. An entirely
613 new 3D-view of the crustal and mantle structure of a South Atlantic passive margin-
614 Santos, Campos and Espírito Santo basins, Brazil. AAPG, Annual Convention and
615 Exhibition, Houston, Abstracts, p. 12.
616
617
618
619 **FIGURE CAPTIONS**

620 **Figure 1**. Geological setting of the East Kirkton Limestone Quarry (red square). Limestones
621 occur interbedded within coeval tuffs and basalt lavas. Location of the studied borehole BH-
622 3 in the study area (modified from Cameron et al, 1998).

623 **Figure 2.**. Main facies types. A) Spherulitic carbonates affected by different scales of soft-
624 sediment deformation. Hammer for scale. B) Spherulitic components are embedded in
625 organic-rich muddy matrices displaying floatstone to laminite textures. C) Spherulites are

composed of fibro-radial calcite generating spherical or elongated particles seen in crossed Nichols. EDS analysis on carbonate spherulites confirms calcite mineralogy (Cc: calcite, Mgc: low-magnesium calcite). D) Floatstone of volcanic remains (Volc) and spherulites (Spher) in a serpentine-like amorphous matrix (Am. silicate). Calcite cements crosscut previous materials. Plane polarized light image. E) Calcite pseudomorphs [Cal and arrows] replacing former amygdaloidal textures [Am] in volcanic rocks. F) Diverse generations of fibroradial/ spherulitic chalcedony [FSC] and drusy mega-quartz cements [DM] as cavity-filling minerals. Dolomite rhombs [D] forming tiny rims around the edge of the cavities.

Figure 3. Borehole BH3 sedimentary log. A) Solid lines show the vertical distribution of the main sedimentologic features. Cross references to figures are written in the log. Key. Sh: Shale, C: Carbonates, V: volcanics.

Figure 4. A) Spherulites are composed of fibro-radial calcite generating spherical or elongated particles seen in cross Nichols. B) Volcanic remains (Volc) and spherulites (Spher) produce a floatstone texture made of clay matrix (Mg/Al clay). Calcite cements (Cem) crosscut previous materials. Plane polarized light image.

Figure 5. A) Thin-section of altered basaltic rock (thin section in plane polarised light). B) Composition maps showing abundance of Ca, Mg, Fe, Al, K elements within the white square on A. C) XRD analysis reveal calcite mineralogy (Cc) for the products filling cavities within altered igneous rocks.

Figure 6. Carbon Preference Indices of n-alkanes from the East Kirkton limestone. Equal concentrations of odd- and even- alkanes (CPI = 1) indicate full thermal maturity. It is these

measurements reflect likely liquid hydrocarbons observed in thin section to have migrated into the pore space, and that these derive from the adjacent West Lothian Oil Shale Formation.

Figure 7. Compilation of Sr isotope data. EK Lst indicates whole rock and HNO_3-soluble fractions of 5 carbonate-rich samples from the East Kirkton Limestone Member. EK leachate / whole rock indicate whole rock and HNO_3-soluble fractions of 3BH1 volcaniclastic samples. Visean Seawater data taken from (Veizer et al., 1999), hydrothermal data taken from (Palmer and Edmond, 1989) Midland Valley Volcanic series data taken from (Smedley, 1986).

Figure 8. Theoretical evolution of the solid mineral assemblage produced by natural hyperalkaline waters from serpentinization during ingassing of CO_2. Note log scale on solid concentration axis, and linear scales otherwise. As ingassing is a progressive process, the X axis can also be read qualitatively as time or distance from source, making vertical sections of the diagram predictions of the mineral assemblage at specific water pH levels.

Figure S1. Facies types and stratigraphic features of the East Kirkton Quarry. A) Laminites display a flat-tabular bedding in outcrop. B) Laminites are composed of an alternation of carbonate-rich (lighter) and organic-rich laminae (darker) and are commonly displaying soft-sediment deformation features (creeping and micro-folding of laminae). C) Plant remains are common in the organic-rich intervals of laminites. D) Greenish to dark orange tuff characterised by a pyroclastic texture with mm-thick angular to subangular lapilli clasts. E)

668 Layered beds formed by an alternation of nodular to tabular limestone beds with organic-
669 rich black clay. Slumps were present. F) Thin section of a spherulitic biohermal carbonate
670 sample displaying the sequential stacking of mm-thick botryoidal calcite fans.

671

SUPPLEMENTARY MATERIAL

PHREEQC MODELLING OF SOLUTION AND MINERAL ASSEMBLAGE COMPOSITION

A simple thermodynamic equilibrium model of reactions between likely spring-water solutions arising from meteoric water serpentinization of alkali igneous rocks was created using PHREEQC Version 3.1.7. Solution composition was drawn from Stanger (1986), who report a large number of springwater compositions from the Oman Mountains. The specific site used was Jalah Spring (site 69 of Stanger, 1986), where waters rise from the middle Harzburgite of the ophiolite series (Dewandel et al., 2005). These rocks and the purely meteoric waters interacting with them provide a close match to the system inferred for East Kirkton, and therefore the solutions produced should be similar in composition. As iron and aluminium composition of these waters are not reported by Stanger 1986, we use representative values for the same region taken from Dewandel et al., (2005). Composition of the initial solution used for the model is shown in Table S1.

This initial solution was allowed to equilibrate with the minerals identified within the East Kirkton Limestone deposit (calcite, dolomite, Mg-smectite, chalcedony). In addition, the high initial pH makes it very likely that Mg-Si phases would be stable under the anticipated conditions of the experiment, so equilibration with a representative mineral (sepiolite) was also permitted (Tosca and Wright, 2015). The charge balance in solution was allowed to freely equilibrate within the parameterization of PHREEQC, and constraint of mineral stabilities was taken from the Laurence Livermore National Laboratory database (llnl.dat).

Once equilibrium between the initial solution and the permitted solid phases has occurred, reaction with gaseous CO_2 was incrementally achieved by sequentially adding 0.01 moles of $CO_{2(g)}$ and calculating the new equilibrium point, including deposition (dissolution) of solid phases. This addition of $CO_{2(g)}$ was continued until calcite became soluble (the abundant calcite present at East Kirkton demonstrates this threshold as not exceeded) or dissolved carbon content of the water reached 1M.

Temperature	34°C
pH	11.4
Al	0.05
Ca	1.530
Cl	11.17
Fe	$4x10^{-5}$
K	0.430
Mg	0.0017
Na	12.706
S	0.081
Si	0.568

Table S1. Composition of initial solution used for modelling. All concentrations are given in millimoles.

Table 1. Strontium isotope data used in this study. Position of samples shown in Figure 3. Results summarised in Figure 7.

Lab No	Sample Name	Sr 87/86	% Std Error	Abs error
H639	BGS 1	0.749678	0.0013	9.74581×10^{-6}
H640	BGS2	0.766026	0.0013	9.95834×10^{-6}
H641	EK 0	0.706511	0.0012	8.47813×10^{-6}
H642	EK 3	0.706817	0.0014	9.89544×10^{-6}
H643	EK 6	0.70685	0.0015	1.06028×10^{-5}
H644	EK 25	0.70764	0.0013	9.19932×10^{-6}
H645	EK 30	0.706706	0.0016	1.13073×10^{-5}
H646	BGS 1WR	0.707575	0.0015	1.06136×10^{-5}
H647	BGS 2WR	0.708487	0.0015	1.06273×10^{-5}
H639 leachate	BGS 1 L	0.706418	0.0017	1.20091×10^{-5}
H640 leachate	BGS 2 L	0.706517	0.0014	9.89124×10^{-5}

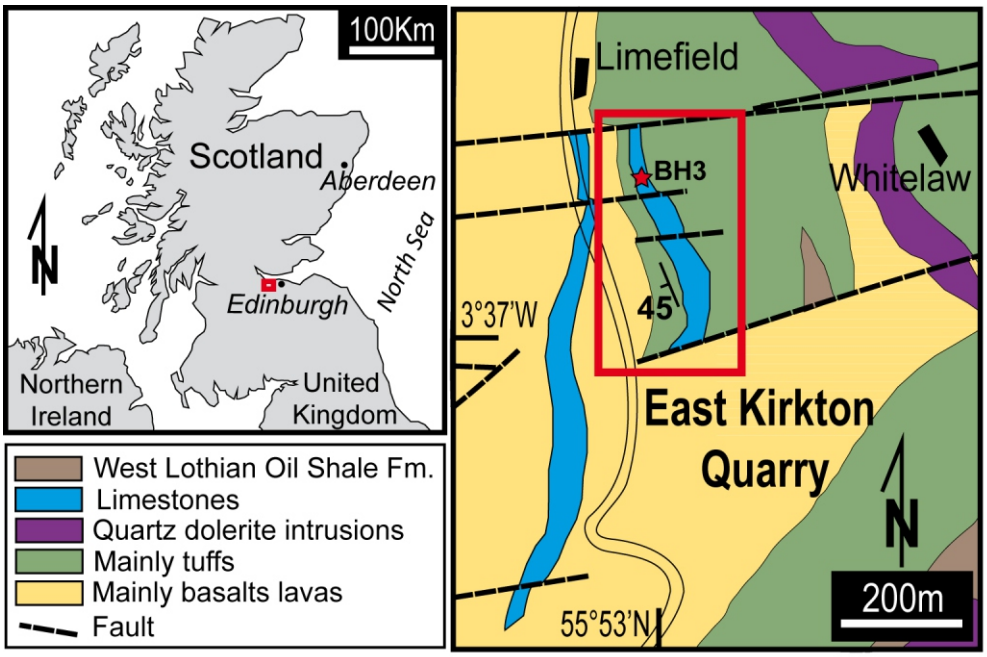
100Km
Scotland
Aberdeen
North Sea
Edinburgh
Northern Ireland
United Kingdom
N
West Lothian Oil Shale Fm.
Limestones
Quartz dolerite intrusions
Mainly tuffs
Mainly basalts lavas
Fault
Limefield
BH3
Whitelaw
45
3°37'W
East Kirkton Quarry
55°53'N
200m

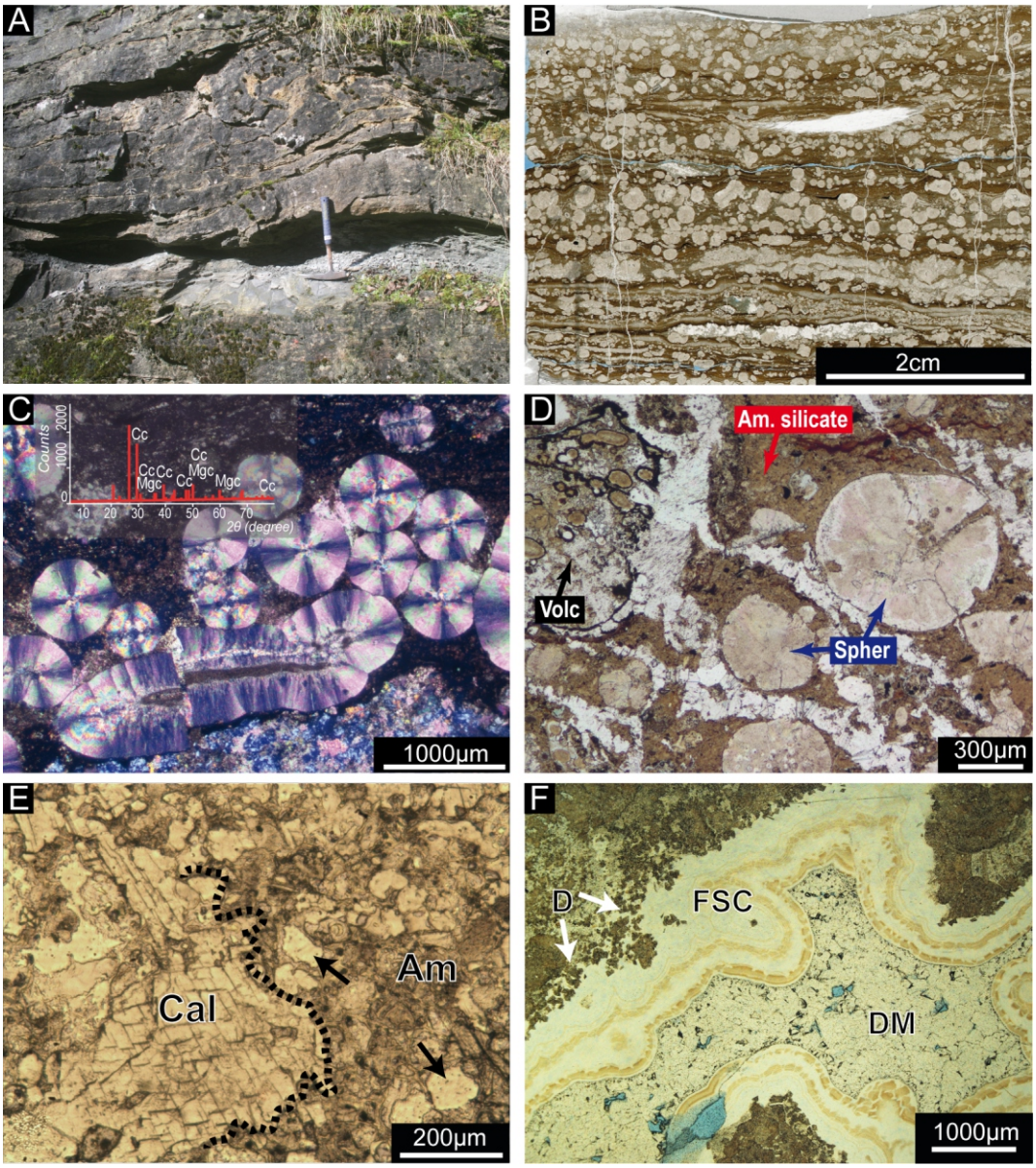
A
B
2cm
C
Counts
2000
1000
0
Cc
Cc
Cc
Mgc
Cc
Cc
Mgc
Mgc
Cc
10
20
30
40
50
60
70
2θ (degree)
1000μm
D
Am. silicate
Volc
Spher
300μm
E
Am
Cal
200μm
F
D
FSC
DM
1000μm

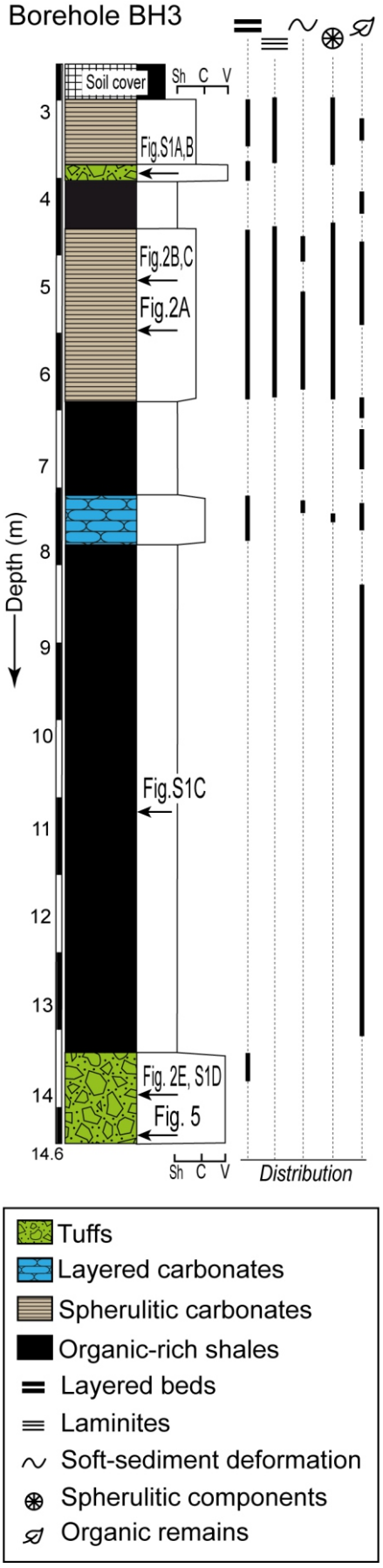
Borehole BH3
Soil cover
Sh C V
Fig.S1A,B
Fig.2B,C
Fig.2A
Fig.S1C
Fig. 2E, S1D
Fig. 5
Depth (m)
3
4
5
6
7
8
9
10
11
12
13
14
14.6
Sh C V
Distribution
Tuffs
Layered carbonates
Spherulitic carbonates
Organic-rich shales
Layered beds
Laminites
Soft-sediment deformation
Spherulitic components
Organic remains

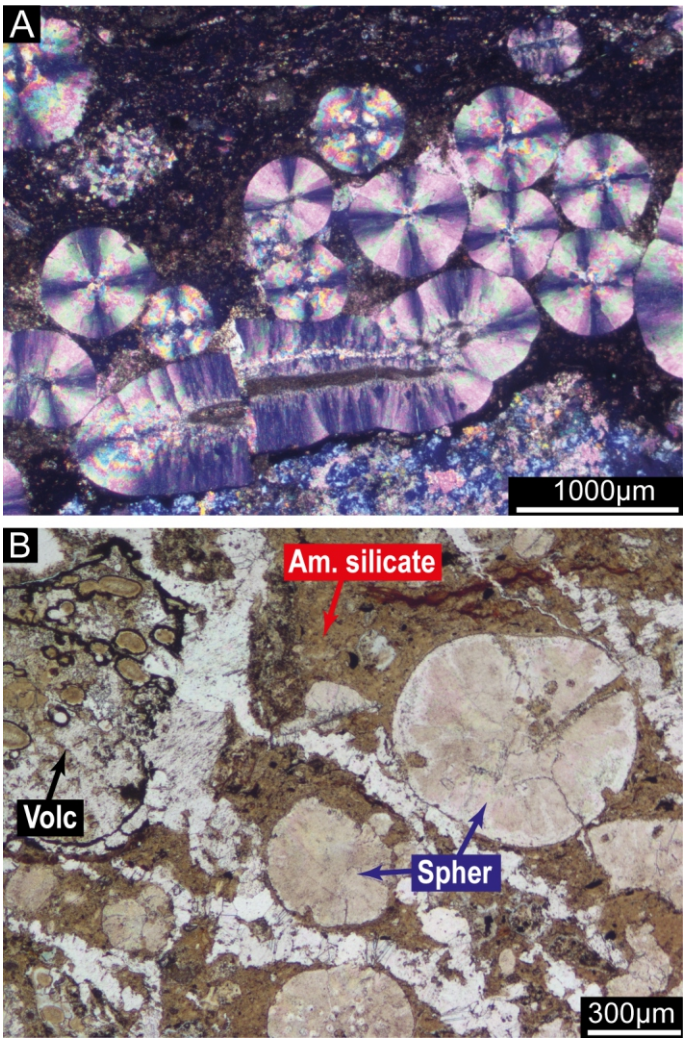
A
1000µm
B
Am. silicate
Volc
Spher
300µm

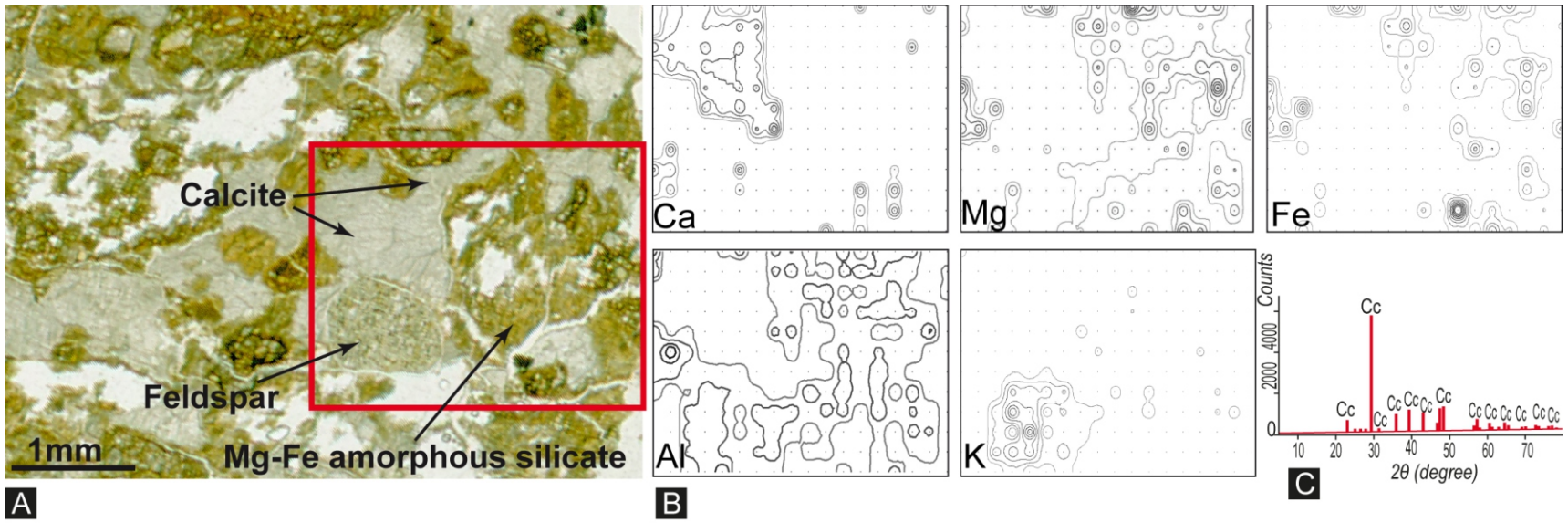
Calcite
Feldspar
Mg-Fe amorphous silicate
1mm
A
Ca
Mg
Fe
Al
K
B
Counts
4000
2000
0
Cc
10
20
30
40
50
60
70
2θ (degree)
C

Figure 6

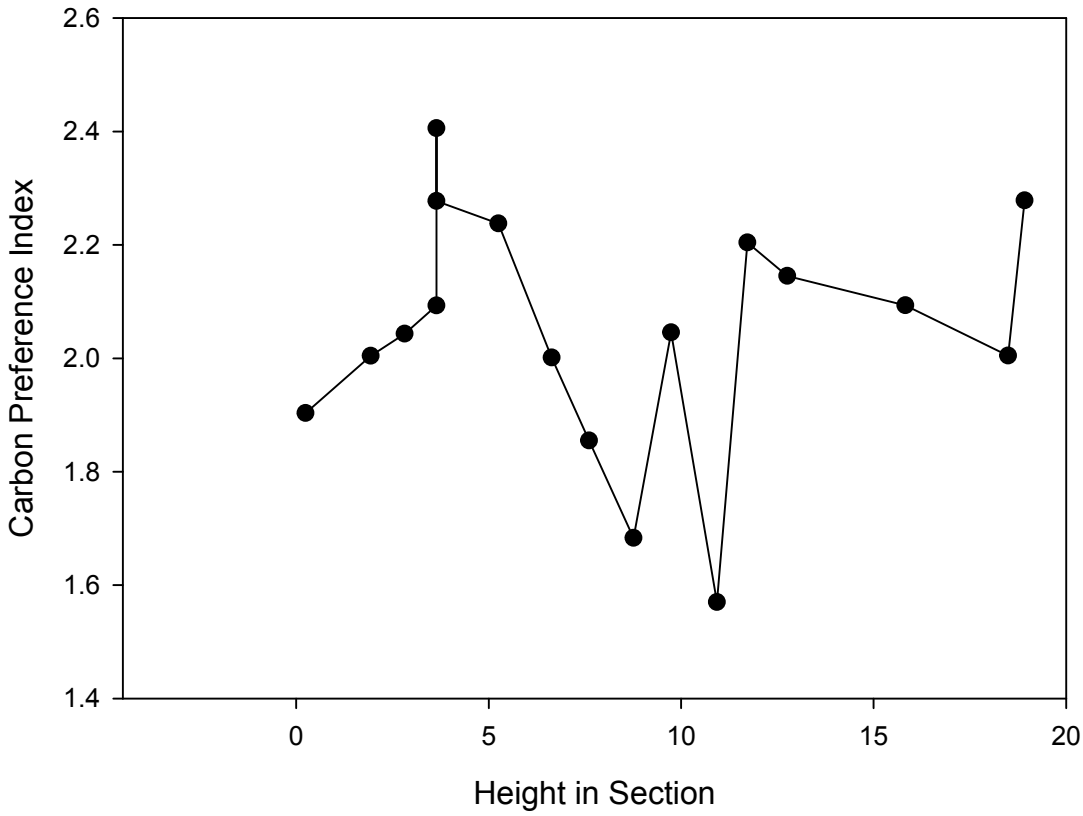
Carbon Preference Index
2.6
2.4
2.2
2.0
1.8
1.6
1.4
0
5
10
15
20
Height in Section

Figure 7

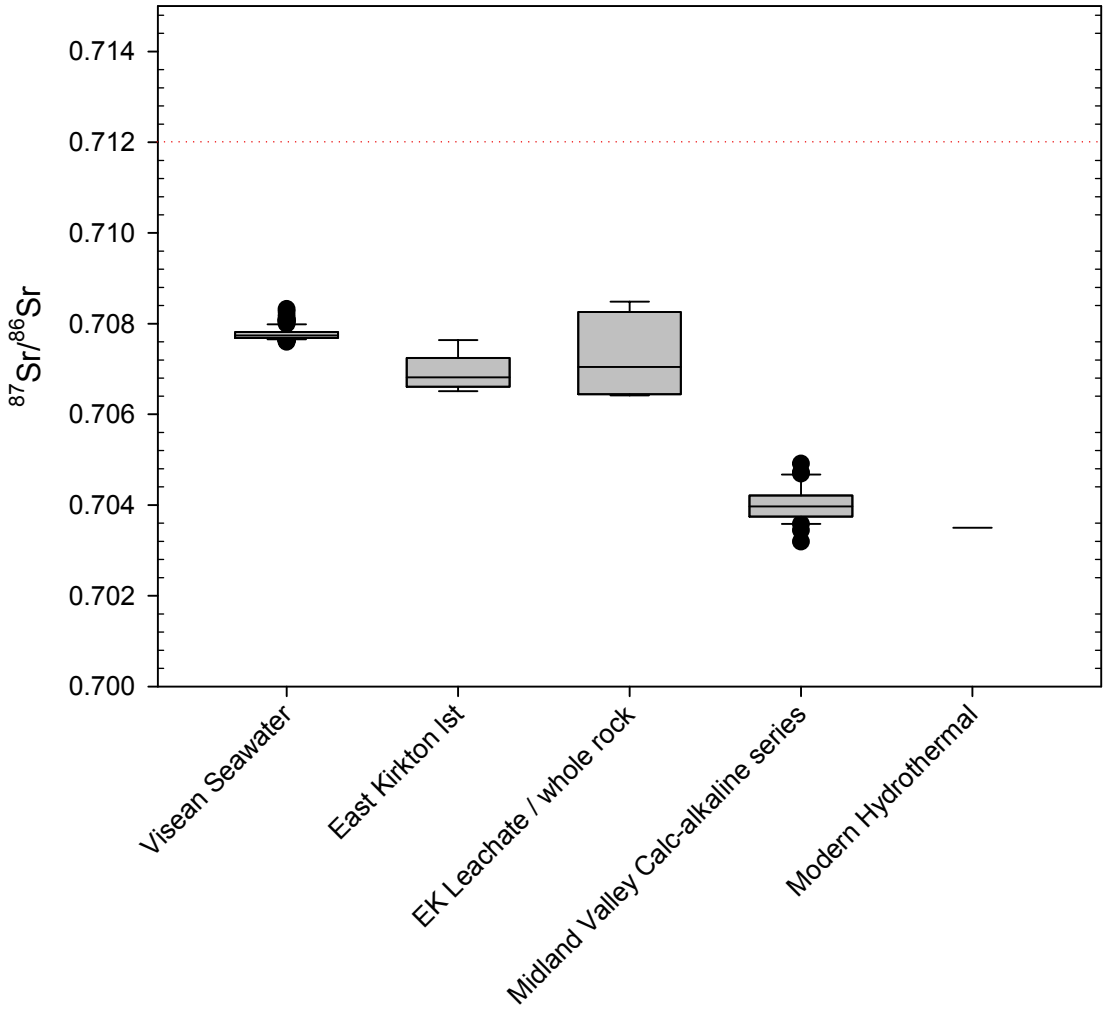
0.714
0.712
0.710
0.708
0.706
0.704
0.702
0.700
$^{87}Sr/^{86}Sr$
Visean Seawater
East Kirkton lst
EK Leachate / whole rock
Midland Valley Calc-alkaline series
Modern Hydrothermal

Figure 8

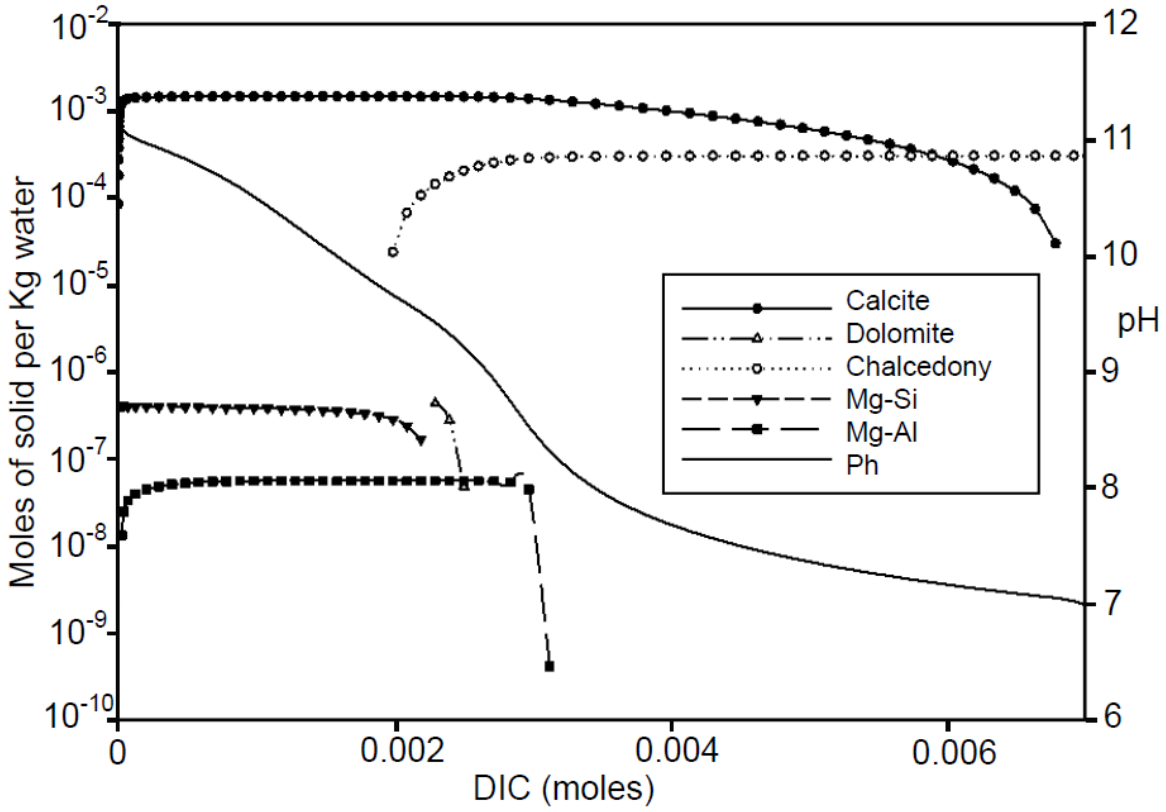
Moles of solid per Kg water
10-2
10-3
10-4
10-5
10-6
10-7
10-8
10-9
10-10
12
11
10
9
8
7
6
pH
0
0.002
0.004
0.006
DIC (moles)
Calcite
Dolomite
Chalcedony
Mg-Si
Mg-Al
Ph

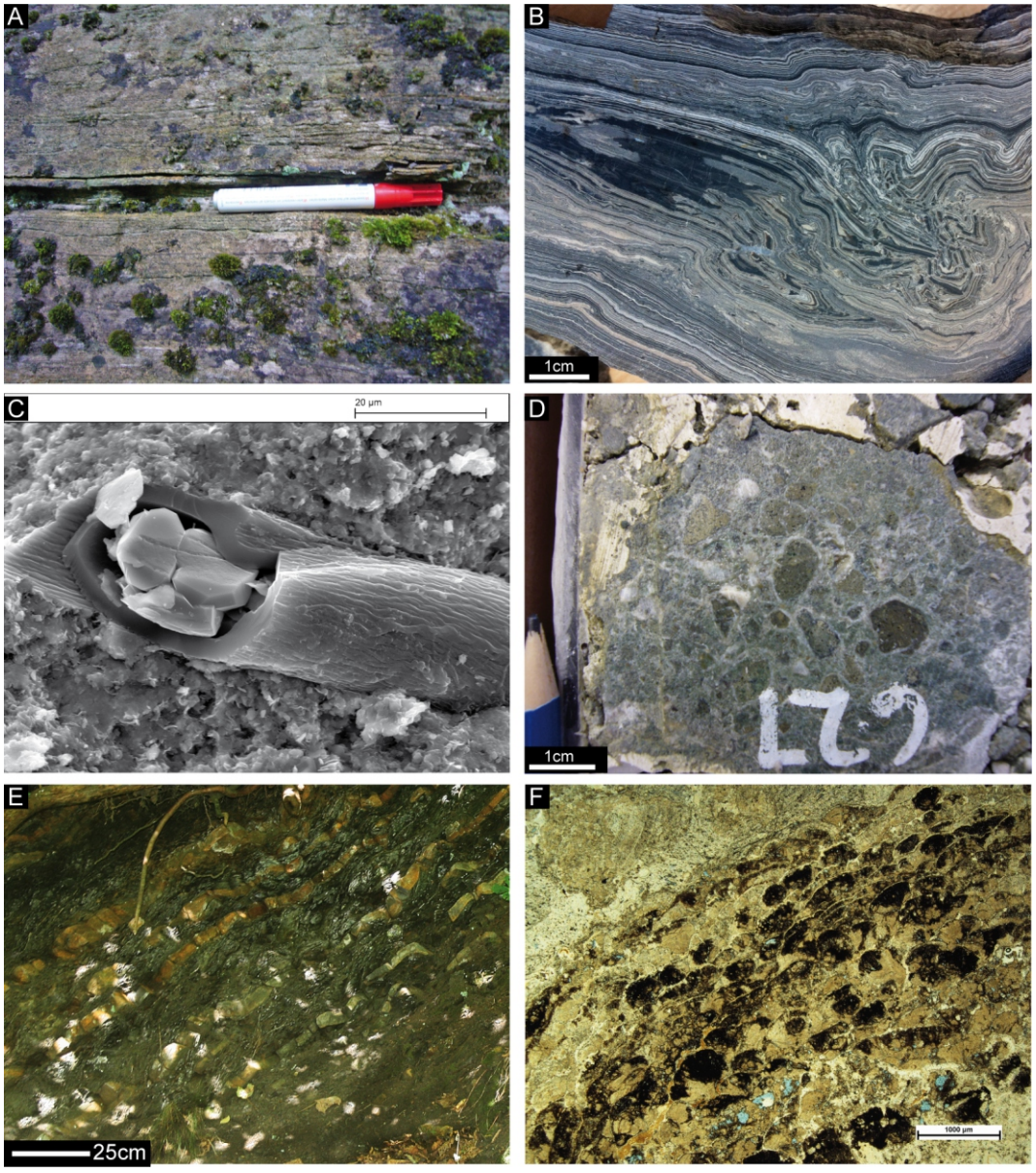
A
B
1cm
C
20 µm
D
1cm
E
25cm
F
1000 µm